ARTICLE

doi:10.1038/nature10246

Second messenger role for Mg^{2+} revealed by human T–cell immunodeficiency

Feng-Yen Li[1,2]*, Benjamin Chaigne-Delalande[1]*, Chrysi Kanellopoulou[1], Jeremiah C. Davis[3], Helen F. Matthews[1], Daniel C. Douek[4], Jeffrey I. Cohen[5], Gulbu Uzel[6], Helen C. Su[3] & Michael J. Lenardo[1]

The magnesium ion, Mg^{2+}, is essential for all life as a cofactor for ATP, polyphosphates such as DNA and RNA, and metabolic enzymes, but whether it plays a part in intracellular signalling (as Ca^{2+} does) is unknown. Here we identify mutations in the magnesium transporter gene, *MAGT1*, in a novel X-linked human immunodeficiency characterized by CD4 lymphopenia, severe chronic viral infections, and defective T-lymphocyte activation. We demonstrate that a rapid transient Mg^{2+} influx is induced by antigen receptor stimulation in normal T cells and by growth factor stimulation in non-lymphoid cells. MAGT1 deficiency abrogates the Mg^{2+} influx, leading to impaired responses to antigen receptor engagement, including defective activation of phospholipase Cγ1 and a markedly impaired Ca^{2+} influx in T cells but not B cells. These observations reveal a role for Mg^{2+} as an intracellular second messenger coupling cell-surface receptor activation to intracellular effectors and identify MAGT1 as a possible target for novel therapeutics.

Mg^{2+} is the most abundant divalent cation in mammalian cells and is an essential cofactor for ATP, nucleic acids, and numerous enzymes in animals and plants[1–3]. Whether it serves as a second messenger in intracellular signalling is controversial[4–8]. Ca^{2+}, another alkaline earth metal, is well-established as a second messenger; this is because the concentration of free intracellular Ca^{2+}, $[Ca^{2+}]_i$, is 0.1 μM and that of free extracellular Ca^{2+}, $[Ca^{2+}]_e$, is 1 mM, creating a steep gradient that favours voltage- and ligand-gated Ca^{2+} influx signals[9]. By contrast, $[Mg^{2+}]_i$ is 10–30 mM and mostly complexed with ATP and other molecules. Only 1–5% (0.2–1 mM) is cytosolic free Mg^{2+}. However, this is 100-fold below its electrochemical equilibrium potential, which theoretically allows regulated Mg^{2+} influxes[6,10]. Mg^{2+} has been found to enhance lymphocyte activation in suboptimal Ca^{2+} concentrations by phytohaemagglutinin (PHA) but not ionomycin[11–13]. As ionomycin bypasses proximal T-cell antigen receptor (TCR) signals, optimal T-cell activation could require a magnesium-generated process upstream of Ca^{2+} signalling. Probes sensitive to Mg^{2+} have revealed changes in $[Mg^{2+}]_i$ in lymphocytes following lectin stimulation[14,15]. Nevertheless, how extracellular Mg^{2+} promotes cellular activation signals is unknown.

The molecular elucidation of primary immunodeficiencies often yields novel insights into lymphocyte signal transduction[16–18]. TCR signalling is critical for T-lymphocyte selection during ontogeny and for peripheral responses against foreign pathogens[19,20]. Mutations in the zeta-chain-associated protein kinase of 70 kDa (ZAP70) tyrosine kinase in severe combined immunodeficiency patients illustrated its role in thymic development of $CD8^+$ T cells and peripheral T-cell activation[19,21]. Likewise, genetic defects in severe combined immunodeficiency patients in ORAI1 revealed that it was a critical store-operated Ca^{2+} channel[22]. Idiopathic CD4 lymphocytopenia (ICL) is a rare immunodeficiency in which circulating $CD4^+$ T-cell counts are $<300\,mm^{-3}$ or <20% of total T cells in the absence of HIV infection or other causes of lymphopenia[23–25]. The aetiology of ICL is heterogeneous, with no infectious cause identified and a genetic aetiology suspected in some cases[26–29]. Here we have uncovered a second messenger role for Mg^{2+} in receptor-induced phospholipase Cγ1 (PLCγ1) activation and Ca^{2+} signalling by discovering an X-linked mutation in *MAGT1*, a highly selective transporter for Mg^{2+}, in a subset of ICL patients.

Immune and gene defects in ICL patients

We examined two young brothers (patients A.1 and A.2) who exhibited recurrent infections, including chronic Epstein–Barr virus infection and low $CD4^+$ T-cell counts; other lymphocyte populations were normal or elevated, and immunoglobulin levels and vaccine responses were only intermittently defective (Supplementary Table 1, Supplementary Fig. 1a, b). Both patients had an inverted CD4:CD8 ratio and reduced $CD31^+$ cells in the naïve ($CD27^+$, $CD45RO^-$) $CD4^+$ T-cell population, suggesting diminished thymic output[30–32] (Fig. 1a, b). However, we also found pronounced defects in TCR-mediated activation events, including CD69, CD25, Fas (CD95) and CTLA-4 upregulation following OKT3 (agonistic anti-CD3) stimulation in peripheral blood mononuclear cells (PBMCs) (Fig. 1c, Supplementary Table 1, Supplementary Fig. 2a). Early TCR signalling events, such as NF-κB and NFAT nuclear translocation, were impaired (Fig. 1e, f). By contrast, the patients' T cells were fully activated by the downstream inducers phorbol 12-myristate 13-acetate (PMA) and ionomycin, implying a proximal TCR activation defect (Fig. 1c, e, f). The patients showed no defect in B-cell receptor (BCR) or toll-like receptor (TLR) stimulation of B cells (Fig. 1d, Supplementary Fig. 2b).

Given that family A harboured two affected boys (Fig. 2a), we tested for X-chromosome linkage by assessing lyonization, the process of X-chromosome inactivation by methylation in females[33]. Skewed lyonization reflects the reduced fitness of cells due to a deleterious X-chromosome mutation. We digested genomic DNA with the methylation-sensitive restriction endonuclease HpaII to eliminate

[1]Molecular Development Section, Lymphocyte Molecular Genetics Unit, Laboratory of Immunology, National Institute of Allergy and Infectious Diseases, National Institutes of Health, Bethesda, Maryland 20892, USA. [2]Biomedical Sciences Graduate Program, University of California-San Francisco, San Francisco, California 94143, USA. [3]Human Immunological Diseases Unit, Laboratory of Host Defenses, National Institute of Allergy and Infectious Diseases, National Institutes of Health, Bethesda, Maryland 20892, USA. [4]Human Immunology Section, Vaccine Research Center, National Institute of Allergy and Infectious Diseases, National Institutes of Health, Bethesda, Maryland 20892, USA. [5]Laboratory of Infectious Diseases, National Institute of Allergy and Infectious Diseases, National Institutes of Health, Bethesda, Maryland 20892, USA. [6]Laboratory of Clinical Infectious Diseases, National Institute of Allergy and Infectious Diseases, National Institutes of Health, Bethesda, Maryland 20892, USA.
*These authors contributed equally to this work.

©2011 Macmillan Publishers Limited. All rights reserved

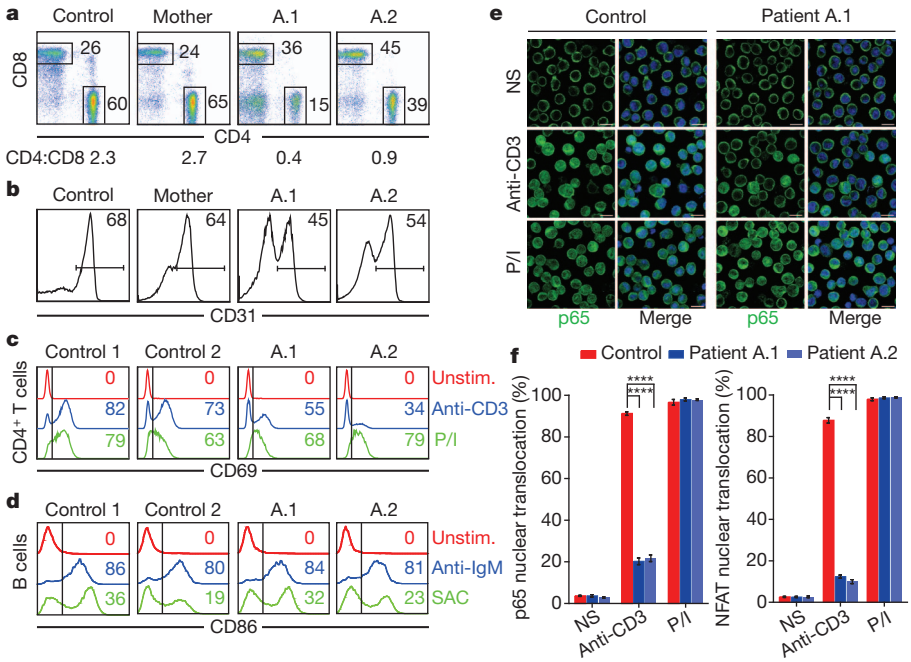

Figure 1 | Patients have a proximal TCR activation defect. **a**, T-cell CD4 and CD8 expression and ratio. **b**, CD31 expression in naïve $CD4^+CD3^+$ T cells. **c**, CD69 expression in $CD4^+$ T cells after 1 μg ml^{-1} anti-CD3 stimulation, PMA/ionomycin (P/I) stimulation or no stimulation (Unstim.). **d**, CD86 expression in purified B cells after stimulation with anti-IgM, SAC or no stimulation. **e**, Confocal imaging of p65 nuclear translocation after anti-CD3 or P/I stimulation or no stimulation (NS) (scale bar, 10 μm). **f**, Percentage of cells with p65 (left) and NFAT (right) nuclear translocation. Numbers represent the percentage of cells in indicated gates. Error bars, s.e.m. ($n = 3$); $^{****}P < 0.0001$.

all active non-methylated X-chromosome DNA and analysed the remaining undigested (inactive) X chromosome by PCR at an indicator locus[33]. The mother of the two affected boys exhibited completely skewed lyonization with only the X chromosome inherited by her two sons inactivated in her T cells, strongly suggesting that she carries an X-linked genetic defect (Fig. 2b).

We therefore performed X-chromosome exon-capture and single-end next-generation sequencing on the mother and the two boys, yielding 18–20 million reads per subject with at least 10× coverage in ~90% of target regions. This revealed a 10-base-pair (bp) deletion in the two brothers present in *MAGT1* (Fig. 2c, Supplementary Fig. 3a), a gene encoding a magnesium transporter[34–36]. This deletion was not detected in the mother's complementary DNA or 100 normal individuals (data not shown). The deletion removes a splice donor site located in the 3′ exon–intron junction of exon 7 and was present in the grandmother and great-grandmother of the patients (Fig. 2a, c, Supplementary Fig. 3a). The patients' mutant *MAGT1* splice variant was ~150 bp smaller than the mother's normal splice variant of approximately 1,100 bp and missing both exon 7 and 8, leading to a premature stop codon (Supplementary Fig. 3b, c). Apparent nonsense-mediated decay caused markedly decreased messenger RNA expression (Fig. 2d). The MAGT1 protein was undetectable in the patients' cells by western blot or immunofluorescent cell surface staining (Fig. 2e, f).

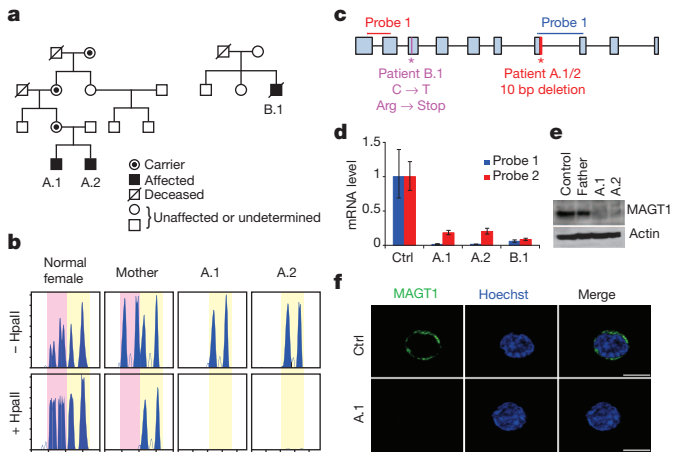

Figure 2 | Patients have MAGT1-null mutations. **a**, Pedigree of the families A (left) and B (right). **b**, X-chromosome inactivation assessed by digestion with (+HpaII) or without (−HpaII) methylation-sensitive enzyme HpaII. Peaks of PCR products from the different alleles are highlighted in yellow and pink. **c**, Schematic representation of the *MAGT1* gene exons (boxes) and introns (lines), the mutations (*) and the probes used for RT–PCR. **d**, RT–PCR showing expression of *MAGT1* mRNA normalized to *HPRT* mRNA in T cells expressed as relative to normal control (CTRL). **e**, Expression of MAGT1 and actin control in T cells by immunoblot. **f**, Confocal images of T cells stained with anti-MAGT1 antibody (scale bars, 5 μm).

Additional screening yielded another immunodeficient patient (B.1) with chronic Epstein–Barr virus infection and a nonsense mutation in exon 3 of *MAGT1*, leading to a 90% decrease in mRNA expression (Fig. 2a, c, d, Supplementary Table 1, Supplementary Fig. 4a). The patient died five years ago from chronic Epstein–Barr virus-associated lymphoma at the age of 45. Like the other two patients, patient B.1 exhibited a similar T-cell defect in NF-κB and NFAT nuclear translocation in response to TCR but not PMA/ionomycin stimulation (Supplementary Fig. 4b, c).

TCR-induced Mg^{2+} and Ca^{2+} influx defects

MAGT1 is a mammalian Mg^{2+}-selective transporter whose physiological function is not well understood[34,35]. The full-length protein of 367 amino acids encodes a signal peptide, a large amino-terminal segment, four transmembrane domains, and a small carboxy-terminal tail with little similarity to any other known transporter except TUSC3, a non-selective Mg^{2+} transporter[36]. We measured ion uptake in normal and patients' lymphocytes using fluorescent probes sensitive for Ca^{2+} (Fluo3-AM and Fura red-AM) or Mg^{2+} (Magfluo4-AM), which exhibited no detectable cross-reactivity (Supplementary Fig. 5a). Initial experiments showed a low basal level

©2011 Macmillan Publishers Limited. All rights reserved

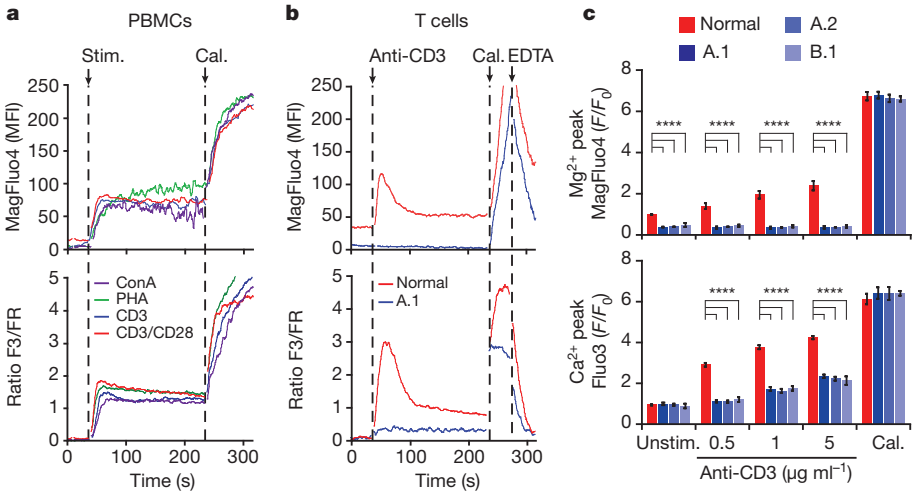

Figure 3 | TCR stimulation induces a MAGT1-dependent Mg^{2+} influx. **a**–**c**, Flux of Mg^{2+} (MagFluo4, upper panels) and Ca^{2+} (ratio Fluo3/Fura Red (F3/FR), lower panels); see Methods for details. MFI, mean fluorescence intensity. **a**, Fluxes in normal PBMCs stimulated (Stim.) with ConA, PHA, anti-CD3, or anti-CD3/anti-CD28. **b**, Fluxes in healthy control T cells or patient A.1 after 1 μg ml^{-1} anti-CD3 stimulation. In **a** and **b**, maximum fluxes were detected with calcimycin (Cal.) treatment to control for dye loading. In **b,** fluxes were quenched with EDTA (EDTA) treatment to show specificity. **c**, Peak value of the fluxes in healthy control T cells and the three patients on stimulation with indicated anti-CD3 concentrations. F/F_0, fluorescence normalized to the value at time 0. Error bars, s.e.m. ($n = 3$); ****$P < 0.0001$.

of free Mg^{2+} and defective passive Mg^{2+} influx, whereas that for Ca^{2+} was normal (Supplementary Fig. 5a). The total Ca^{2+} and Mg^{2+} levels in the patients' T cells determined by inductively coupled plasma mass spectrometry were normal, indicating that MAGT1 deficiency chiefly affects free Mg^{2+} and that general metabolic processes requiring bound Mg^{2+} should not be affected (Supplementary Fig. 5b).

We next examined whether various TCR stimuli would affect free Mg^{2+} transport. We observed a robust transient Mg^{2+} influx together with the well-documented Ca^{2+} influx in normal PBMCs stimulated with various TCR agonists (Fig. 3a). The apparent Mg^{2+} influx was not due to cross-detection of the Ca^{2+} influx, because the specific Ca^{2+} chelator 1,2-bis(*o*-aminophenoxy)ethane-N,N,N′,N′-tetraacetic acid acetoxymethyl ester (BAPTA-AM) abolished the Ca^{2+} fluorescence but not the Mg^{2+} fluorescence (Supplementary Fig. 6a). The Mg^{2+} influx was not detectable in the patients' T cells even with the strongest TCR agonist tested (5 μg ml^{-1} anti-CD3) (Fig. 3b, c). Surprisingly, we also found that the Ca^{2+} influx was severely compromised in the patients' T cells across a broad dose range of anti-CD3 stimulation (Fig. 3b, c). The TCR-induced Mg^{2+} influx was selective, as stimulation of T cells with secondary lymphoid tissue chemokine (SLC/CXCL21), Fas-ligand (FasL) and tumour necrosis factor-α (TNFα) caused no Mg^{2+} influx and the Ca^{2+} influxes induced by SLC and FasL were normal in the patient's cells (Supplementary Fig. 6b). Also, no Mg^{2+} influx was discernible in B lymphocytes following anti-IgM and anti-CD40 stimulation, and the ensuing Ca^{2+} influx was not diminished in patients' B cells (Supplementary Fig. 6c). Although the patients' B cells exhibited reduced basal free Mg^{2+}, their B-cell activation was normal (Fig. 1d).

We next examined the hypothesis that the defective Ca^{2+} influx in the patients was secondary to the loss of the Mg^{2+} influx. We first explored the relationship between the TCR-stimulated influxes in normal T cells by modulating $[Mg^{2+}]$ and $[Ca^{2+}]$ in the extracellular buffer. Both Mg^{2+} and Ca^{2+} influxes were optimal when $[Mg^{2+}]_e$ and $[Ca^{2+}]_e = 1$ mM, respectively, but were abolished when $[Mg^{2+}]_e$ and $[Ca^{2+}]_e = 0$, respectively (Fig. 4a). Moreover, when $[Mg^{2+}]_e = 0$, the Ca^{2+} influx was decreased, but when $[Ca^{2+}]_e = 0$, the Mg^{2+} influx was unaffected (Fig. 4a). These results show that the TCR-induced Ca^{2+} influx is partially dependent on $[Mg^{2+}]_e$. Thus, we infer that the Ca^{2+} influx defect in T cells associated with MAGT1 deficiency is secondary to the loss of the TCR-stimulated Mg^{2+} influx. Conversely, when $[Mg^{2+}]_e = 0$, the Ca^{2+} influx in B cells after the BCR stimulation is normal, which is consistent with the absence of BCR-induced Mg^{2+} influxes (Fig. 4b, Supplementary Fig. 6b). Thus, the loss of the TCR-induced Ca^{2+} influx in the absence of extracellular Mg^{2+} is not likely to be due to a deficiency in Mg^{2+} as a cofactor required for ATP-dependent processes, as B cells had no comparable defect. This is underscored by the fact that both B and T cells from the MAGT1-deficient patients had the same partial reduction in the free $[Mg^{2+}]_i$, but only the latter exhibited functional defects in antigen receptor signalling.

To determine whether Mg^{2+}-promoted Ca^{2+} influxes are important in other tissues, we treated two transformed epithelial cell lines, A549 and HepG2, with epidermal growth factor (EGF), which is known to cause a PLCγ1-dependent Ca^{2+} influx analogous to that induced by TCR engagement[37]. In each cell type, we observed a clear

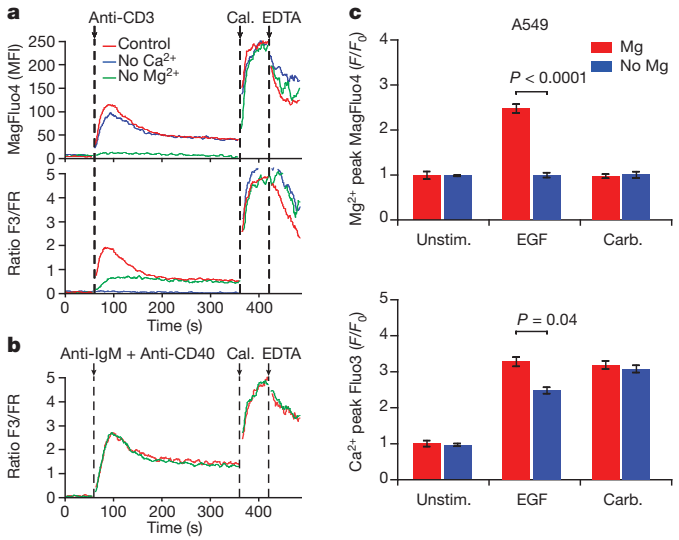

Figure 4 | Requirement of receptor-stimulated Mg^{2+} influx for Ca^{2+} influx. **a**, Mg^{2+} (MagFluo4, upper panel) and Ca^{2+} (ratio F3/FR, lower panel) flux in healthy control T cells stimulated with anti-CD3 in buffers containing 1 mM Mg^{2+} and Ca^{2+} (control) or lacking either ion. **b**, Ca^{2+} flux in B cells stimulated with anti-IgM and anti-CD40. In **a** and **b**, calcimycin (Cal.) and EDTA addition display maximum influx and ion chelation, respectively. **c**, Graphs represent the fold change of the peak of Mg^{2+} (upper panels) and Ca^{2+} (lower panels) flux in A549 cells either unstimulated (Unstim.) or stimulated with epidermal growth factor (EGF) or carbachol (Carb.). Error bars, s.e.m. ($n = 3$).

©2011 Macmillan Publishers Limited. All rights reserved

dose-dependent influx of Mg^{2+} induced by EGF that was abrogated when $[Mg^{2+}]_e = 0$ (Fig. 4c, Supplementary Fig. 7). The EGF-induced Ca^{2+} influx was also decreased, though not abolished, by Mg^{2+} depletion. By contrast, carbachol, an agonist for acetylcholine receptors that induces a Ca^{2+} influx through PLCβ, failed to induce a Mg^{2+} influx. In addition, the carbachol-induced Ca^{2+} influx was not altered when $[Mg^{2+}]_e = 0$. Thus, receptor-induced Mg^{2+} influxes that promote Ca^{2+} influxes occur in both lymphoid and non-lymphoid tissue types. Moreover, receptors that trigger a Ca^{2+} influx through PLCγ1, but not PLCβ or PLCγ2 (BCR), can induce a Mg^{2+} influx to regulate the Ca^{2+} influx.

Knockdown and reconstitution of MAGT1

To demonstrate that decreased MAGT1 expression can account for the immunological and signalling defects observed in the patients, we knocked down MAGT1 in normal human T cells by transient short interfering RNA (siRNA) transfections. We found that the TCR-stimulated Mg^{2+} and Ca^{2+} influxes were decreased in proportion with the degree of *MAGT1* mRNA knockdown (Fig. 5a, Supplementary Fig. 8a). Similar to the patients' T-cell phenotype, MAGT1 knockdown impeded TCR-induced p65 nuclear translocation (Fig. 5b, Supplementary Fig. 8b). These results verify that MAGT1 is necessary for normal T-cell activation.

To determine whether MAGT1 deficiency is sufficient to explain the patients' functional defects, we reconstituted MAGT1 expression by lentiviral transduction of patient T cells. Positively transduced cells marked by a coexpressed fluorescent marker (mCherry) were examined by live cell confocal imaging of the influxes. We found that expressing wild-type MAGT1 in the patients' T cells restored a TCR-stimulated Mg^{2+} influx (Fig. 5c). MAGT1 restoration also improved the TCR-stimulated Ca^{2+} influx, thereby validating our conjecture that it is contingent on the Mg^{2+} influx (Fig. 5c). The expression of MAGT1 also augmented other activation events of the patients' T cells, such as TCR-induced CD69 upregulation (Fig. 5d). Thus, MAGT1 is necessary and sufficient for the Mg^{2+} influx required for optimal T-cell activation,

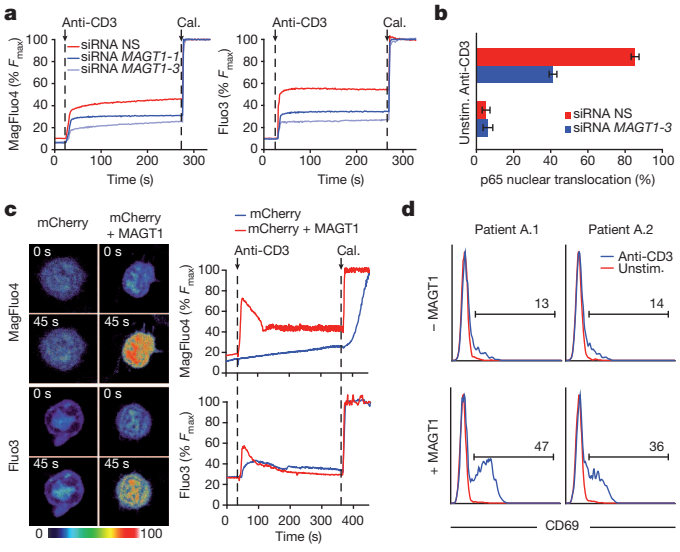

Figure 5 | Knockdown and rescue of MAGT1. Healthy T cells transfected with non-specific (NS) or *MAGT1* siRNAs. **a**, Mg^{2+} (MagFluo4, left) and Ca^{2+} (Fluo3, right) flux upon anti-CD3 stimulation. **b**, Percentage of nuclear p65 after MAGT1 knockdown. Error bars represent s.e.m. ($n = 3$). **c**, Time-lapse imaging (left; time shown in seconds) or cytometry (right) of Mg^{2+} (upper) and Ca^{2+} (lower) flux in T cells transduced with lentiviruses expressing mCherry or mCherry + MAGT1. **d**, Flow cytometry of CD69 expression on $CD4^+$ T cells transduced with lentiviruses expressing MAGT1 or not and either unstimulated (Unstim.) or stimulated with anti-CD3. Percentage of cells are shown for the indicated gates. Calcimycin (Cal.) addition displays maximum influx. % F_{max}, fluorescence normalized as percentage of the maximum value.

and MAGT1 deficiency is the proximate cause of the T cell activation defect in this primary immunodeficiency.

Loss of MAGT1 impairs PLCγ1 activation

To understand the molecular mechanism of the Ca^{2+} influx defect observed in MAGT1-deficient patients, we examined proximal TCR signalling components (Fig. 6d). TCR engagement causes clustering and phosphorylation of the CD3ζ chain by the Src-family leukocyte-specific protein tyrosine kinase (Lck) and subsequent recruitment of the protein tyrosine kinase ZAP70, which phosphorylates the scaffold proteins linker of activated T cells (LAT) and Src homology 2 (SH2) domain-containing leukocyte protein of 76 kDa (SLP76)[20,38]. These phosphorylated scaffolds then bind inducible T cell kinase (Itk), which activates PLCγ1 and thereby generates inositol triphosphate (IP_3) and diacylglycerol (DAG) as second messengers to trigger Ca^{2+} mobilization and protein kinase Cθ (PKCθ) activation, respectively. The Ca^{2+} influx modulates the protein phosphatase calcineurin, which, together with PKCθ, activates downstream transcription factors such as NF-κB and NFAT[39]. We found that TCR cluster formation and LAT and PLCγ1 recruitment to these clusters were intact in patient T cells after anti-CD3 stimulation (Fig. 6a, Supplementary Fig. 9). Moreover, early TCR activation events including the phosphorylation of CD3ζ, Lck, ZAP70 and LAT induced by TCR ligation were normal in the patient's T cells using flow cytometric staining (Supplementary Fig. 10) and western blots (Fig. 6b). Again, this normal series of activation events excludes a general defect in Mg^{2+} as a co-factor for ATP-requiring processes accounting for the TCR signalling defects in MagT1-deficient T cells. By contrast, PLCγ1 activation was markedly delayed by almost one hour in the patient T cells compared to healthy control T cells (Fig. 6b). Moreover, the activating phosphorylation of PKCθ and IP_3 generation downstream of PLCγ1 were significantly reduced (Fig. 6b, c). On the other hand, we found that TCR signalling events that do not require PLCγ1, such as the phosphorylation of the mitogen activated protein kinases (MAPKs) p38 and Erk1/2, were intact in the patient T cells (Fig. 6b). This deficiency in PLCγ1 and PKCθ activation following TCR stimulation was recapitulated by RNAi silencing of *MAGT1* in normal T lymphocytes (Supplementary Fig. 11). Thus, Mg^{2+} can regulate signal transduction pathways involving PLCγ1 in lymphoid and non-lymphoid cells, and MAGT1-deficiency profoundly delays the activation of the PLCγ1 branch of TCR signalling.

Discussion

We have found a biologically important transient Mg^{2+} influx mediated by MAGT1 during T-cell activation and EGF stimulation of epithelial cells. Three fundamental features of a second messenger have been put forward[40]: (1) its levels must increase rapidly in response to a stimulus, which is typically the engagement of a cell-surface receptor (first messenger), (2) it needs to alter the rate of one or more cellular processes, and (3) it exerts cell-type specific activity because different cells harbour different complements of enzymes. We find that Mg^{2+} fulfils these requirements and is a kinetic regulator of signalling in T cells. We found no difference in total Mg^{2+} content between our patients and healthy controls, indicating that MAGT1 does not influence general Mg^{2+} homeostasis or its cofactor function. Rather, we measured rapid and transient free Mg^{2+} influxes after TCR engagement which depends on the MAGT1 transporter. These transient Mg^{2+} influxes increased the rate of PLCγ1 activation and the corresponding Ca^{2+} influx in T cells. B cells, which depend on PLCγ2 for the BCR-induced Ca^{2+} influx, have no such requirement for MAGT1-mediated Mg^{2+} influxes despite their expression of MAGT1. Because ions diffuse rapidly as second messengers, a Mg^{2+} influx may promote rapid spatial integration of antigen and costimulatory receptor signals critical for T-cell activation. Our findings shed new light on older observations that extracellular magnesium promotes lymphocyte activation synergistically with calcium by T-cell, but not B-cell,

©2011 Macmillan Publishers Limited. All rights reserved

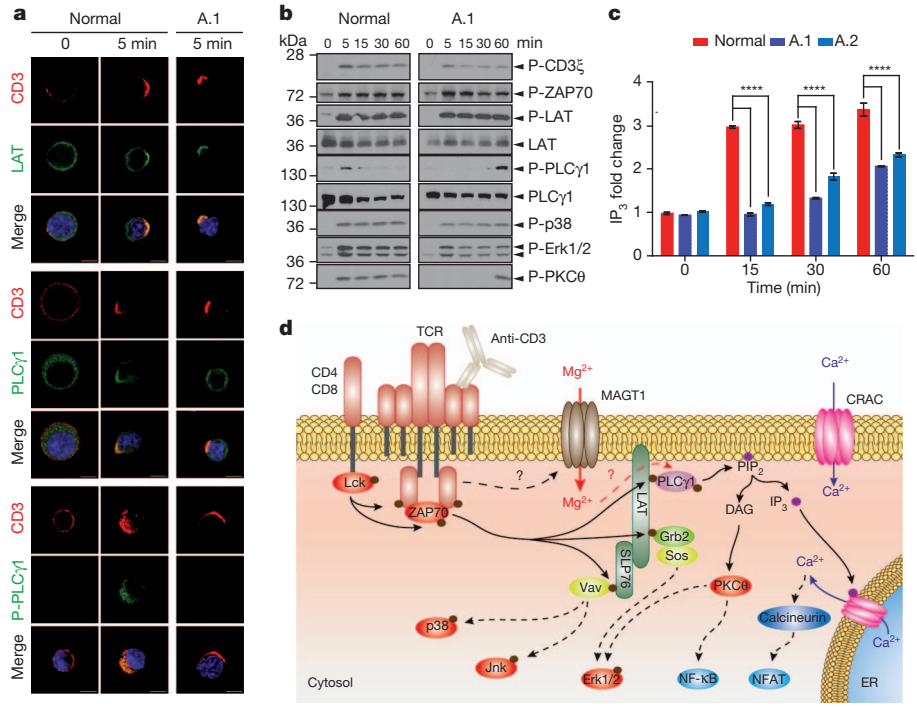

Figure 6 | MAGT1 deficiency impairs PLCγ1 activation upon TCR stimulation. **a**, Confocal images of TCR clustering induced by anti-CD3. Cells were stained for LAT, PLCγ1 or phospho (P)-PLCγ1. Scale bar, 5 μm. **b**, **c**, Immunoblot of the indicated signalling proteins and phosphoproteins (**b**) and quantification of cellular IP_3 level (**c**) in healthy control and patient's T cells stimulated with anti-CD3 for indicated times. Error bars, s.e.m. ($n = 3$); $^{****}P < 0.0001$. **d**, Hypothetical schematic depicting how the MAGT1-mediated Mg^{2+} influx participates in TCR signalling. Solid arrows indicate direct effects; dashed arrows indicate indirect effects. ER, endoplasmic reticulum.

mitogens, and that mice fed Mg^{2+}-deficient diets have lower calcineurin activity in their splenocytes[11–13,41,42]. It will also be of interest to determine if defective thymopoiesis caused by disruption of the TRPM7 Mg^{2+} channel could be due to the loss of the signalling function of Mg^{2+} influxes[43].

The patients examined in this study have a novel X-linked primary immunodeficiency impairing thymic production of $CD4^+$ T cells and circulating T-cell function which we now denominate XMEN (X-link immunodeficiency with magnesium defect and Epstein–Barr virus infection and neoplasia) disease. The defective development and function of T cells in XMEN patients categorizes them as T cell immunodeficiency patients, although they have a mild phenotype comprising chiefly uncontrolled viral infections consistent with a T-cell-specific defect[44]. They also share features with X-linked lymphoproliferative disease (XLP) except for the absence of NKT cell deficits or haemophagocytic lymphohistiocytosis[45]. Like XMEN patients, mice with PLCγ1-deficient T cells have fewer $CD4^+$ T cells and defective TCR activation, but they also have features that we did not observe in the patients, such as impaired ERK activation, lower numbers of $CD8^+$ T cells and $FoxP3^+$ regulatory T cells, and inflammatory/autoimmune symptoms[46]. The fact that XMEN patients only have a kinetic block in PLCγ1 activation, whereas the mice have a complete deficiency, could account for these differences.

Finally, the integrity of early TCR activation events in the patients' T cells explains how MAGT1 acts as a TCR-gated transporter that controls a new step in the later contingent series of TCR signalling events[47] (Fig. 6d). The selective requirement of this Mg^{2+} influx for the activation of T cells but not B cells suggests that MAGT1 may be a useful therapeutic target for diseases requiring T-cell-specific immunomodulation.

METHODS SUMMARY

All human subjects in this study provided informed consent in accordance with Helsinki principles to be enrolled in research protocols approved by the institutional review board of the National Institute of Allergy and Infectious Diseases, NIH. Patients' and healthy control PBMCs were Ficoll-purified and activated with anti-CD3 and anti-CD28 for 3 days and then continuously cultured in 10% RPMI media supplemented with 100 U ml^{-1} IL-2 for 3–4 weeks. For assessment of primary stimulation, cells were collected and stained with anti-CD2, anti-CD4 and anti-CD8 antibodies, and various activation markers for 30 min at 4 °C and analysed with a FACS Calibur or a LSRII flow cytometer (BD Biosciences). Activated T cells were restimulated with various T-cell activation agents, and processed for immunofluorescence imaging, immunoblotting and influx assays, as described in Methods. Genomic DNA isolated from activated T cells was prepared for lyonization assays, SureSelect Human X Chromosome (Agilent) target enrichment, single-read Solexa sequencing on Illumina Genome Analyser IIx, and Sanger sequencing according to the manufacturer's instructions. All *P* values were calculated with the Student's *t*-test using PRISM software (GraphPad Software), with a two-tailed distribution.

Full Methods and any associated references are available in the online version of the paper at www.nature.com/nature.

Received 30 March; accepted 3 June 2011.

1. Cakmak, I. & Kirkby, E. A. Role of magnesium in carbon partitioning and alleviating photooxidative damage. *Physiol. Planta* **133,** 692–704 (2008).
2. Cowan, J. A. Structural and catalytic chemistry of magnesium-dependent enzymes. *Biometals* **15,** 225–235 (2002).
3. Yang, W., Lee, J. Y. & Nowotny, M. Making and breaking nucleic acids: two-Mg^{2+}-ion catalysis and substrate specificity. *Mol. Cell* **22,** 5–13 (2006).
4. Gasser, A., Bruhn, S. & Guse, A. H. Second messenger function of nicotinic acid adenine dinucleotide phosphate revealed by an improved enzymatic cycling assay. *J. Biol. Chem.* **281,** 16906–16913 (2006).
5. Grubbs, R. D. & Maguire, M. E. Magnesium as a regulatory cation: criteria and evaluation. *Magnesium* **6,** 113–127 (1987).
6. Murphy, E. Mysteries of magnesium homeostasis. *Circ. Res.* **86,** 245–248 (2000).
7. Permyakov, E. A. & Kretsinger, R. H. Cell signaling, beyond cytosolic calcium in eukaryotes. *J. Inorg. Biochem.* **103,** 77–86 (2009).
8. Takaya, J., Higashino, H. & Kobayashi, Y. Can magnesium act as a second messenger? Current data on translocation induced by various biologically active substances. *Magnes. Res.* **13,** 139–146 (2000).
9. Hogan, P. G., Lewis, R. S. & Rao, A. Molecular basis of calcium signaling in lymphocytes: STIM and ORAI. *Annu. Rev. Immunol.* **28,** 491–533 (2010).
10. Romani, A. M. Magnesium homeostasis in mammalian cells. *Front. Biosci.* **12,** 308–331 (2007).

©2011 Macmillan Publishers Limited. All rights reserved

11. Abboud, C. N., Scully, S. P., Lichtman, A. H., Brennan, J. K. & Segel, G. B. The requirements for ionized calcium and magnesium in lymphocyte proliferation. *J. Cell. Physiol.* **122,** 64–72 (1985).
12. Modiano, J. F., Kelepouris, E., Kern, J. A. & Nowell, P. C. Requirement for extracellular calcium or magnesium in mitogen-induced activation of human peripheral blood lymphocytes. *J. Cell. Physiol.* **135,** 451–458 (1988).
13. Whitney, R. B. & Sutherland, R. M. The influence of calcium, magnesium and cyclic adenosine 3′,5′-monophosphate on the mixed lymphocyte reaction. *J. Immunol.* **108,** 1179–1183 (1972).
14. Ng, L. L., Davies, J. E. & Garrido, M. C. Intracellular free magnesium in human lymphocytes and the response to lectins. *Clin. Sci. (Lond.)* **80,** 539–547 (1991).
15. Rijkers, G. T. & Griffioen, A. W. Changes in free cytoplasmic magnesium following activation of human lymphocytes. *Biochem. J.* **289,** 373–377 (1993).
16. Chun, H. J. *et al.* Pleiotropic defects in lymphocyte activation caused by caspase-8 mutations lead to human immunodeficiency. *Nature* **419,** 395–399 (2002).
17. Notarangelo, L. D. Primary immunodeficiencies. *J. Allergy Clin. Immunol.* **125,** S182–S194 (2010).
18. Zhang, Q. *et al.* Combined immunodeficiency associated with DOCK8 mutations. *N. Engl. J. Med.* **361,** 2046–2055 (2009).
19. Chan, A. C. *et al.* ZAP-70 deficiency in an autosomal recessive form of severe combined immunodeficiency. *Science* **264,** 1599–1601 (1994).
20. Peterson, E. J. & Koretzky, G. A. Signal transduction in T lymphocytes. *Clin. Exp. Rheumatol.* **17,** 107–114 (1999).
21. Arpaia, E., Shahar, M., Dadi, H., Cohen, A. & Roifman, C. M. Defective T cell receptor signaling and $CD8^+$ thymic selection in humans lacking zap-70 kinase. *Cell* **76,** 947–958 (1994).
22. Feske, S. *et al.* A mutation in Orai1 causes immune deficiency by abrogating CRAC channel function. *Nature* **441,** 179–185 (2006).
23. Unexplained CD4+ T-lymphocyte depletion in persons without evident HIV infection — United States. *MMWR Morb. Mortal. Wkly. Rep.* **41,** 541–545 (1992).
24. Laurence, J., Siegal, F. P., Schattner, E., Gelman, I. H. & Morse, S. Acquired immunodeficiency without evidence of infection with human immunodeficiency virus types 1 and 2. *Lancet* **340,** 273–274 (1992).
25. Smith, D. K., Neal, J. J. & Holmberg, S. D. Unexplained opportunistic infections and CD4+ T-lymphocytopenia without HIV infection. An investigation of cases in the United States. *N. Engl. J. Med.* **328,** 373–379 (1993).
26. Fauci, A. S. CD4+ T-lymphocytopenia without HIV infection — no lights, no camera, just facts. *N. Engl. J. Med.* **328,** 429–431 (1993).
27. Freier, S. *et al.* Hereditary CD4+ T lymphocytopenia. *Arch. Dis. Child.* **78,** 371–372 (1998).
28. Lin, S. J., Chao, H. C., Yan, D. C. & Kuo, M. L. Idiopathic CD4+ T lymphocytopenia in two siblings. *Pediatr. Hematol. Oncol.* **18,** 153–156 (2001).
29. Lobato, M. N., Spira, T. J. & Rogers, M. F. CD4+ T lymphocytopenia in children: lack of evidence for a new acquired immunodeficiency syndrome agent. *Pediatr. Infect. Dis. J.* **14,** 527–535 (1995).
30. Junge, S. *et al.* Correlation between recent thymic emigrants and CD31+ (PECAM-1) CD4+ T cells in normal individuals during aging and in lymphopenic children. *Eur. J. Immunol.* **37,** 3270–3280 (2007).
31. Kimmig, S. *et al.* Two subsets of naive T helper cells with distinct T cell receptor excision circle content in human adult peripheral blood. *J. Exp. Med.* **195,** 789–794 (2002).
32. Kohler, S. & Thiel, A. Life after the thymus: CD31+ and CD31− human naive CD4+ T-cell subsets. *Blood* **113,** 769–774 (2009).
33. Wengler, G. S. *et al.* A PCR-based non-radioactive X-chromosome inactivation assay for genetic counseling in X-linked primary immunodeficiencies. *Life Sci.* **61,** 1405–1411 (1997).
34. Goytain, A. & Quamme, G. A. Identification and characterization of a novel mammalian Mg^{2+} transporter with channel-like properties. *BMC Genomics* **6,** 48–66 (2005).
35. Quamme, G. A. Molecular identification of ancient and modern mammalian magnesium transporters. *Am. J. Physiol. Cell Physiol.* **298,** C407–C429 (2010).
36. Zhou, H. & Clapham, D. E. Mammalian MagT1 and TUSC3 are required for cellular magnesium uptake and vertebrate embryonic development. *Proc. Natl Acad. Sci. USA* **106,** 15750–15755 (2009).
37. Xie, Z., Peng, J., Pennypacker, S. D. & Chen, Y. Critical role for the catalytic activity of phospholipase C-γ1 in epidermal growth factor-induced cell migration. *Biochem. Biophys. Res. Commun.* **399,** 425–428 (2010).
38. Weiss, A. & Littman, D. R. Signal transduction by lymphocyte antigen receptors. *Cell* **76,** 263–274 (1994).
39. Nel, A. E. T-cell activation through the antigen receptor. Part 1: signaling components, signaling pathways, and signal integration at the T-cell antigen receptor synapse. *J. Allergy Clin. Immunol.* **109,** 758–770 (2002).
40. Sutherland, E. W. Studies on the mechanism of hormone action. *Science* **177,** 401–408 (1972).
41. Flynn, A. Control of *in vitro* lymphocyte proliferation by copper, magnesium and zinc deficiency. *J. Nutr.* **114,** 2034–2042 (1984).
42. Sabbagh, F., Lecerf, F., Hulin, A., Bac, P. & German-Fattal, M. Effect of hypomagnesemia on allogeneic activation in mice. *Transpl. Immunol.* **20,** 83–87 (2008).
43. Jin, J. *et al.* Deletion of Trpm7 disrupts embryonic development and thymopoiesis without altering Mg^{2+} homeostasis. *Science* **322,** 756–760 (2008).
44. Cossu, F. Genetics of SCID. *Ital. J. Pediatr.* **36,** 36–76 (2010).
45. Filipovich, A. H., Zhang, K., Snow, A. L. & Marsh, R. A. X-linked lymphoproliferative syndromes: brothers or distant cousins? *Blood* **116,** 3398–3408 (2010).
46. Fu, G. *et al.* Phospholipase Cγ1 is essential for T cell development, activation, and tolerance. *J. Exp. Med.* **207,** 309–318 (2010).
47. Crabtree, G. R. Contingent genetic regulatory events in T lymphocyte activation. *Science* **243,** 355–361 (1989).

Supplementary Information is linked to the online version of the paper at www.nature.com/nature.

Acknowledgements We thank L. Zheng, A. Weiss, R. Germain, R. Siegel, F. Wolf and P. Schwartzberg for critically reading the manuscript; F. Wolf for advice on magnesium assessments; L. Zheng, C. Lowell and A. Weiss for advice on experiments and data; H. Jing for making HVS lines from patient cells; P. Chen for assistance with plasmid DNA preparation; N. Sandler for flow cytometry assistance; A. Snow and H. Jing for assistance with genomic DNA library preparation for Solexa sequencing; J. Almenara and Illumina staff for Solexa assistance; D. Killilea for assistance with MS-ICP data interpretation; and A. Irani for referring the patients. F.-Y.L. is in the Medical Scientist Training Program at the University of California–San Francisco and thanks K. Shannon and J. Toutolmin for support and encouragement. This work was supported by the Division of Intramural Research of the National Institute of Allergy and Infectious Diseases of the US National Institutes of Health.

Author Contributions F.-Y.L. characterized the MAGT1 mutations and the TCR activation defect in the patients. B.C.-D. characterized the Mg^{2+} influx and the signalling defects. B.C.-D., F.-Y.L., H.C.S. and M.J.L. conceived and planned the experiments, and prepared the manuscript. J.C.D. performed the lyonization assay. C.K. performed the RT–PCR experiments. G.U., J.I.C. and H.C.S. referred patients and provided clinical data. H.F.M. coordinated clinical protocol and sample collection. D.C.D. provided assistance with sequencing and flow cytometry, and guided some patient assessments. All authors discussed and revised the manuscript.

Author Information The Illumina sequencing data has been deposited in dbGaP with accession code phs000365.v1.p1. Reprints and permissions information is available at www.nature.com/reprints. The authors declare no competing financial interests. Readers are welcome to comment on the online version of this article at www.nature.com/nature. Correspondence and requests for materials should be addressed to M.J.L. (lenardo@nih.gov).

©2011 Macmillan Publishers Limited. All rights reserved

METHODS

Cells and reagents. PBMCs were isolated from whole blood by Ficoll-Hypaque (GE Healthcare) density gradient centrifugation, washed, and resuspended at 10^6 cells ml^{-1} in complete RPMI 1640 medium (Lonza) containing 10% fetal calf serum (FCS), 2 mM glutamine, and penicillin and streptomycin (100 U ml^{-1} each, Invitrogen). T cells were activated with 1 μg ml^{-1} each of anti-CD3ε and anti-CD28 monoclonal antibodies (BD Biosciences) or with 0.8 ng ml^{-1} PMA (Sigma) and 0.4 μM ionomycin (Sigma). After 3 days, activated T cells were washed and then cultured in complete RPMI-1640 medium supplemented with 100 U ml^{-1} rhIL-2 (R&D). B cells were enriched by negative selection using a B cell isolation kit II (Miltenyi).

Antibodies against p65 (RelA), phospho-PKCθ (S695) and phospho-CD3ζ (C415.9A) were from Santa Cruz. Antibodies against CD4, CD8, CD31, CD40, CD69, CD86, hIgM and phospho-Lck (Y394) were from BD Bioscience. Antibodies against phospho-LAT (Y191), LAT, phospho-PLCγ1 (Y783), PLCγ1, phospho-p38 and phospho-Erk1/2 (T202/204) were from Cell Signaling Technology. ConA and PHA were from Sigma. Recombinant FasL and TNFα were from Alexis and recombinant SLC was from PeproTech. All flow cytometry staining and analysis were performed using standard protocols[18,48].

Lyonization assay. Lyonization assays were adapted from ref. 49. Briefly, genomic DNA (1 μg) samples were first digested with RsaI (NEB) and then split into two for treatment with or without HpaII (NEB). Each digestion was carried out for at least 2 h and heat inactivated at 65 °C for 20 min. Digested DNA was purified by QIAquick PCR purification kit (Qiagen) and PCR amplified using 6-FAM-conjugated primers for the HUMARA locus: 5′-TGCGCGAAGTGATC CAGAACC-3′, 5′-TGGGCTTGGGGAGAACCATCC-3′. The amplified products were analysed on a 310 Gene Analyser (ABI) as recommended using ROX500 (ABI) as size standard.

Exome sequencing and analysis. Genomic DNA isolated from T cells by DNeasy Blood and Tissue kit (Qiagen) was processed using Genomic DNA Sample Prep Kit (Illumina) for SureSelect Human X Chromosome (Agilent) target enrichment according to manufacturer instructions. Captured DNA was subject to cluster generation using Single-Read Cluster Generation Kit v2 (Illumina) and massive parallel sequencing using SBS Sequencing Kit v3 (Illumina) on the Illumina Genome Analyser IIx. The data were imported into CLCbio Genomics Workbench software and aligned to the human genome reference (hg19) annotated with SNPs (130) downloaded from UCSC Genomics browser. Detection of SNPs and deletion insertion polymorphisms (DIPs) was performed on alignments in the software, and genes with missing coverage were identified using the targeted resequencing plug-in tool (CLCbio). Candidate genes were filtered using available filters on the software and in Excel spreadsheets. Sanger sequencing was performed as described previously[18].

From the Illumina sequencing data, all single nucleotide polymorphisms (SNPs) and 1–2 bp DIPs that were not present in both brothers, not heterozygous in the mother, or that were found in her cDNA were excluded. Large DIPs (>1 kb) were screened by using comparative genomic hybridization 244K arrays (Agilent) as described previously[18]. To detect 3–1,000 bp DIPs, the targeted resequencing plug-in tool (CLCbio) was used to identify genes with missing coverage in the patients but not in the mother. SNPs and DIPs consistent with these search criteria were ruled out as common polymorphisms in the normal population by Sanger sequencing 100 normal controls.

Transfection and transduction. Full-length *MAGT1* was PCR amplified from normal control T-cell cDNA and subcloned into the BamI and NotI restriction sites of LeGO-iG[50] plasmid and into XhoI and BamHI restriction sites of the pLenti-bicistronic (Applied Biological Materials, ABM) plasmid. mCherry was also subcloned into the SnaBI and NotI restriction sites of pLenti-bicistronic plasmid. These constructs were each cotransfected with lentiviral second generation packaging mix (ABM) in 1:1 mix into HEK293T (70% confluent) using Turbofect transfection reagent (Fermentas). After 2 days, virus supernatants were harvested and concentrated by overnight ultracentrifugation at 20,000*g* at 4 °C. Virus pellets were resuspended in 10% RPMI and stored at −80 °C. Unstimulated PBMCs purified from whole blood by Ficoll were transduced using virus made from LeGO-iG as described[10]. Three days after transduction, half of the transduced PBMCs were activated with 1 μg ml^{-1} OKT3 and analysed for activation by flow cytometry. Day 4 stimulated T cells were transduced similarly using virus made from pLenti-bicistronic vector. Two days after transduction, cells were harvested for influx measurements by confocal imaging.

For RNAi gene silencing of *MAGT1*, total T cells purified by Pan T cell isolation kit (Miltenyi Biotech) were transfected using P3 Primary Cell 4D-Nucleofector X kit (Lonza) with either Stealth RNAi Negative Control Duplexes or Stealth siRNA targeting *MAGT1* (Invitrogen): si*MAGT1-1* (5′-GCCCAAAGAAAGAAGGAGA UGGUGU-3′), si*MAGT1-3* (5′-UCAUGUUCACUGCUCUCCAACUGCA-3′). Transfected cells were cultured in 10% RPMI media for at least 4 h before stimulation with 1 μg ml^{-1} each of anti-CD3 and anti-CD28 for 48 h. Transfection was repeated again with the same siRNA, and transfected cells were cultured in 10% RPMI media supplemented with 100 U ml^{-1} rhIL-2 for 48–72 h. Subsequently, cells were harvested for fluorimetric influx measurements and microscopic assessment of p65 translocation following stimulation with OKT3 or PMA/ionomycin. At the same time, cells were processed for real-time assessment of *MAGT1* mRNA expression using Taqman Gene Expression Assays (ABI).

Confocal imaging. For nuclear translocation of p65 and NFAT, cells were stimulated with either OKT3 or PMA/ionomycin for 30 min. Then cells were dropped on poly-L-lysine coated slides and fixed with 3% paraformaldehyde in phosphate-buffered saline (PBS), permeabilized with 0.05% Triton X-100 for 3 min at room temperature, and blocked with PBS containing 10% FCS. For TCR clustering, activated peripheral blood lymphocytes (PBL) from normal control and patient were incubated on ice with anti-CD3 antibody (1 μg ml^{-1}) for 30 min, washed and stained with Alexa-568 goat anti-mouse antibody for 30 min. Cell were then incubated at 37 °C for indicated times on poly-L-lysine coated slides and then fixed and permeabilized. All slides were stained with indicated primary antibody in 0.5% BSA-PBS for 45 min at room temperature. Slides were washed and incubated with an Alexa 488-conjugated donkey anti-rabbit antibodies (Invitrogen) for 45 min. Nuclei were stained with Hoechst 33342 (50 ng ml^{-1}, Invitrogen). Slides were washed in PBS, rinsed, and mounted with a coverslip using Fluoromount-G (Southern Biotechnology). All images were collected on a Leica TCS-NT/SP5 confocal microscope (Leica Microsystems) using a 63× oil immersion objective NA 1.32, 'zoom X'. For enumeration of percentage of cells with nuclear NF-κB, NFAT or CD3 clustering, 450–700 cells were scored visually by a single observer.

Calcium and magnesium flux experiments. Cells were loaded with 1 μM Magfluo4-AM (Invitrogen) or 1 μM Fluo3-AM (Invitrogen) and 1 μM Fura Red-AM (Invitrogen) for 20 min at 37°C. Then, cells were washed in incubation buffer (IB: 120 mM N-methyl-D-glucamine, 20 mM HEPES, 4.7 mM KCl, 1.2 mM KH_2PO_4, 10 mM glucose, pH 7.4) with or without 1.2 mM $CaCl_2$ and/or 1.2 mM $MgSO_4$. The loading efficiency was assessed by adding 1 μM calcimycin, a Ca^{2+}/Mg^{2+} ionophore that causes large influxes of both ions. For flow cytometry experiments, intracellular calcium and magnesium were measured using a BD LSRII flow cytometer. Kinetic analyses used the FlowJo software package (TreeStar), with percentage of responding cells defined as >95th percentile of unstimulated baseline. For fluorimeter experiments, cells were seeded in a 96-well plate and assessed with a POLARstar OPTIMA plate reader (BMG LabTech). For confocal microscopy, cells were plated on LabTek II Chamber Slide (Nunc) coated with 0.01% poly-L-lysine, and analysed with a Leica TCS-NT/SP5 confocal microscope (Leica Microsystems) using a 63× oil immersion objective NA 1.32, 'zoom X'.

Immunoblotting. Activated T cells were starved for 4 h in RPMI medium without FCS. Then cells were stimulated with OKT3 (1 μg ml^{-1}) for indicated times. Stimuli were terminated by addition of ice-cold PBS, and pelleted cells were immediately lysed in 1% Triton X-100, 1% NP40, 50 mM Tris pH 8, 150 mM NaCl, 20 mM EDTA, 1 mM Na_3VO_4, 1 mM NaF, phophatase inhibitor cocktail (Sigma) and complete protease inhibitor cocktail (Roche). Protein concentration was quantitated by BCA assay (Pierce). 30 μg of cell lysates were separated by SDS–PAGE and transferred on PVDF membrane (Millipore). Membrane was blocked with BSA for 1 h before incubating with primary antibodies overnight. HRP-conjugated secondary antibodies were from Southern Biotechnology. Pierce Supersignal West chemiluminescent substrates were used for detection. MAGT1 blotting was performed on unstarved activated T cells using 1:1,000 anti-MAGT1 (Proteintech).

Quantitative total elemental content measurement. 10 million $CD8^+$ T cells purified from PBMCs using human CD8 Microbeads (Miltenyi Biotech) were stimulated with anti-CD3 and anti-CD28 for 3 days and subsequently cultured continuously in 10% RPMI media with 100 U ml^{-1} IL-2 at ~1–2 million cells per ml. When sufficient cells accumulated, duplicate aliquots of 5, 10 and 15 million cells were pelleted and dried overnight at 32 °C. Total magnesium, calcium and sulphur content was measured for each cell pellet by inductively coupled plasma mass spectrometry as described[51]. Similar results for Mg^{2+} were obtained for $CD4^+$ T cells (data not shown).

IP_3 measurement. IP_3 levels from stimulated T cells were assessed using an IP_3 ELISA kit (Cusabio) according manufacturer's instructions.

Statistical analysis. *P* values were calculated with the Students *t*-test using PRISM software (GraphPad Software), with a two-tailed distribution.

48. Petrovas, C. *et al.* PD-1 is a regulator of virus-specific CD8+ T cell survival in HIV infection. *J. Exp. Med.* **203,** 2281–2292 (2006).
49. Allen, R. C., Zoghbi, H. Y., Moseley, A. B., Rosenblatt, H. M. & Belmont, J. W. Methylation of HpaII and HhaI sites near the polymorphic CAG repeat in the human androgen-receptor gene correlates with X chromosome inactivation. *Am. J. Hum. Genet.* **51,** 1229–1239 (1992).
50. Weber, K., Bartsch, U., Stocking, C. & Fehse, B. A multicolor panel of novel lentiviral "Gene Ontology" (LeGO) vectors for functional gene analysis. *Mol. Ther.* **16,** 698–706 (2008).
51. Killilea, D. W. & Ames, B. N. Magnesium deficiency accelerates cellular senescence in cultured human fibroblasts. *Proc. Natl Acad. Sci. USA* **105,** 5768–5773 (2008).

©2011 Macmillan Publishers Limited. All rights reserved